

Chapter 4

Crustal imaging in southern California using earthquake sequences

4.1 Introduction

Acoustic imaging using the tools of exploration seismology and earthquake sources allows us to produce reflection views of the crust at depths where other data are commonly not available. For instance, James et al. (1987) and Meyer and James (1987) obtained near-vertical reflection profiles in regions of shallow seismicity, and Spudich and Bostwick (1987) capitalized on the principle of seismic reciprocity to form apparent receiver arrays from earthquake clusters, allowing them to derive apparent velocity information from just a few stations recording many events.

Morales and McMechan (1990) illustrated earthquake source imaging based on finite-difference extrapolation, and reviewed the acoustic and elastic cases. They found that, in principle, earthquake recordings allow for reconstruction of source properties, locations, and fault orientations. Also, Rietbrock and Scherbaum (1994) described numerical examples and a successful case of a well-focused acous-

tic image of one earthquake source.

James et al. (1987) described some of the inherent difficulties and limitations that have discouraged the use of earthquake sources for reflection imaging. Nevertheless, there has been considerable interest in passive seismic imaging in the past few years due to the expansion of regional seismic networks, which have recorded digital seismograms from hundreds of stations. For instance, analyses of scattered waves using stacking and Kirchhoff migration have proven useful in the evaluation of generalized site effects and earthquake hazard (Spudich and Miller, 1990; Spudich and Iida, 1993; Revenaugh, 1995a, b, c; Revenaugh and Mendoza, 1996), as well as in studies of crustal scatterers near small-aperture arrays (Hedlin et al., 1994) and lower mantle heterogeneities (Lay and Young, 1996), taking advantage of a limited range of scattering angle in those data sets.

Despite this recent work, earthquake seismologists may still be reluctant to believe that one can image faults successfully using only $P - P$ scattering characteristics, as I do here. For instance, Aki (1992) showed that $P - S$ conversion for seismic waves is much greater than $S - P$. Thus, the dominance of S -waves in the coda of seismograms raises concern about the validity of dealing with $P - P$ scattering in imaging deep crustal reflectors. $P - S$ converted waves dominate the P -wave coda for teleseismic events, and $S - P$ converted waves greatly contribute to the P -coda waves of regional earthquakes (Matsumoto, 1995). Thus, the mode conversion problem is inherently troublesome in earthquake seismology, and this remains the case in seismic reflection imaging.

In the context of exploration seismology, in which sources are typically either explosive or vertical vibrators, and recording apertures are small relative to the target depths, the effects of source directivity are less crucial (Chen and McMechan, 1992) than in earthquake seismology. Crustal-scale wide-angle experiments are potentially more affected by source type because of the wider range of propagation angles involved. Source directivity differences become increasingly important at wider and wider apertures. Strong source directivity does indeed affect the imaging process, but I show that it does not hinder the reconstruction of fault geometries having reflectivities normally associated with deep-crustal structures.

As in oil industry seismic-reflection surveying, imaging of structure through high-frequency reflectivity demands high-multiplicity data, or a large number of overlapping sources and receivers. Despite the intrinsic limitations of close source spacing (within an aftershock sequence) and wide station spacing, my initial work (Chávez-Pérez and Louie, 1995) showed that a small cluster of tens of aftershocks has the spatial sampling needed to image crustal reflectors beneath the Northridge aftershock zone. In the case of the Northridge earthquake, the close spatial distribution of aftershocks illuminates structures not previously mapped at depth (e.g., Hauksson et al., 1995). A reliable velocity structure over the three-dimensional array of sources (aftershocks) and receivers (network stations) provides some of the information needed to locate crustal reflectors in cross sections or 3-D volumes.

Locating crustal reflectors has important neotectonic implications because the proper development of earthquake scenarios for southern California requires dis-

covering the location and character of known and still unknown fault structures (e.g., Hauksson, 1990; Shaw and Suppe, 1996). Prime examples of blind thrusts are the sources of the 1983 Coalinga, 1987 Whittier Narrows, and 1994 Northridge earthquakes in California. Seismological evidence for the Northridge mainshock fault mechanism, the focal mechanisms and the spatial distribution of aftershocks (Hauksson et al., 1995) are consistent both with thin-skinned (Davis and Nanson, 1994) and thick-skinned (Huftile and Yeats, 1996) hypotheses for blind-thrust faulting in southern California.

I test the applicability of these models using aftershock recordings to obtain images of crustal structure. This chapter describes imaged structure beneath the 1991 Sierra Madre and 1994 Northridge earthquake sequences, using aftershocks treated with simple data editing and Kirchhoff depth migration.

4.2 Data selection and preprocessing

The ideal sources for performing crustal imaging would be underground explosions, due to their simple focal mechanism (Lay, 1987; Lynnes and Lay, 1989). Successful Kirchhoff summation depends upon consistent focal mechanisms or a source correction. Here, I have made no correction for the source but, for the sake of attaining coherent summations, I use only data with high-quality impulsive P -wave picks to roughly correct for sign reversals due to varying focal mechanisms and source directivity, where the scattered ray paths have takeoff angles close to the

direct ray takeoff angle. (In future work, I may improve these summations by using events with the same focal mechanism.) My data are short-period vertical-component seismograms from the SCSN provided through the Southern California Earthquake Center (SCEC) Data Center. I use well-located, A-quality events.

It is worth mentioning that the SCSN is one of the best seismic networks in the USA and in the world. Its data are critical to the evaluation of earthquake hazards in southern California and to the advancement of geoscience as a whole (Wald, 1996). The SCSN provides one of the best receiver arrays in the world. Its data quality and quantity may be the highest anywhere.

Clipped and saturated records are quite common in short-period data. I regard them as sign-bit recordings (O'Brien et al., 1982) that will acquire dynamic range through Kirchhoff summation. To project a reflected wave from a seismogram to a reflector location one needs to know the time of the arrival, and be able to characterize it as having significant amplitude within the seismogram. Stacking and migration find events that have some coherency across a source-receiver array (of events in this case) and sum amplitudes to reject uncorrelated noise. I can thus obtain coherent reflections, for instance, by common midpoint stacking (Chávez-Pérez and Louie, 1995) to improve the signal-to-noise ratio, or even by simple vertical stacking. With sufficient data redundancy, stacking and migration are often able to recover geometric information.

The record sections I use comprise up to 200 km epicentral distance and 30 s duration to include wide-angle reflections between first compressional (P_g) and

first shear (S_g) arrivals, and I mute outside the window between the approximate P_g and S_g traveltimes to extract only compressional arrivals, mostly some unmuted P_g , P_mP and $S - P$ converted energy. Of course, imaging artifacts result from not muting completely the direct P_g arrivals. As they have the minimum arrival time at any offset, they will contaminate the shallow part of the images. This is not too important for me as I am interested in deep, mid-crustal structures. In addition, I must include forward-scattered energy with traveltimes close to the P_g arrival time.

Despite the fact that the bulk of short-period earthquake data analyses deal with the frequency band of 1-10 Hz, I chose to retain a wider spectrum. I retain a frequency band of 1-40 Hz because the spectra of my signals show some energy above the noise level for frequencies above 10 Hz. This is also the frequency range where reflections normally associated with deep-crustal structures have predominated in active-source crustal studies (e.g., Brewer and Oliver, 1980). In addition, there is implicit low-pass filtering during the migration process, and one can always remove the effects of high-frequency noise from the images, for plotting and stacking purposes, by postmigration low-pass or dip filtering to enhance visibility and resolution. Thus, preprocessing includes bandpass filtering (1-40 Hz) and trace equalization for receiver amplitude balancing (i.e., the amplitudes are normalized so that the mean-squared amplitude over the $P_g - S_g$ window of each trace is the same for all traces). This is roughly equivalent to energy normalization for varying magnitudes, and geometrical spreading correction, as discussed in Chapter 3.

4.3 Results

4.3.1 Sierra Madre earthquake sequence

Using seismic network recordings of the 1991 Sierra Madre event and its aftershocks (Hauksson, 1994), I undertook the imaging of a section through the San Gabriel Mountains near the Los Angeles Region Seismic Experiment (LARSE) Line 1, in an attempt to reproduce a lower crustal bright spot seen by Fuis et al. (1996). The stack of explosion seismograms presented by Fuis et al. (1996) shows an outstanding, high-amplitude band of reflectivity, a “lower crustal reflective zone” (LCRZ), at approximately 16 to 19 km (between 5.5 and 6.5 s, two-way travel time) beneath the San Gabriel Mountains, between Azusa in San Gabriel Valley and the San Andreas fault near Wrightwood, and extending about 25 km laterally (Ryberg et al., 1996).

Fig. 4.1 shows the locations of LARSE Line 1 and section A that I used to depict a 50-km-long by 40-km-deep image of crustal structure in this region. The N-S orientation of section A traverses major structures in the area, and is also for computational convenience. Fig. 4.2 shows a representative aftershock plotted as a reduced-time record section independent of azimuth. Note the azimuthal time dependence of the impulsive P_g arrivals. Arrows depict expected traveltimes for one diffractor located within the lower crustal reflective zone of Fuis et al. (1996). Fig. 4.3 shows the same record section in Fig. 4.2 after bandpass filtering. Some of the expected traveltimes are a bit easier to follow, but it is difficult to define

ch4f1.ps

Figure 4.2: Example vertical-component record section from one Sierra Madre aftershock (hypocentral depth = 9.3 km). Impulsive P_g arrivals are clear. The data are plotted as a function of reduced traveltime versus offset of the recording station, independent of azimuth. Trace equalization was used for the display. Arrows depict expected traveltimes for one diffractor located within the lower crustal reflective zone of Fuis et al. (1996).

Figure 4.3: Example vertical-component record section from one Sierra Madre aftershock (hypocentral depth = 9.3 km). Impulsive P_g arrivals are clear. The data were bandpass filtered (1-10 Hz) and are plotted as a function of reduced travelttime versus offset of the recording station, independent of azimuth. Trace equalization was used for the display. Arrows depict expected traveltimes for one diffractor located within the lower crustal reflective zone of Fuis et al. (1996).

lateral continuity of the traveltimes due to the azimuthal time dependence.

According to Fuis et al. (1996), the top of the lower-crustal reflective zone represents a “block boundary,” or change in rock properties, in the crustal framework of southern California. They proposed that the top may be a décollement or an intrusive contact. In fact, the depth to the brittle-ductile transition seems to be prescribed by the existence of reflective structures like this (Magistrale and Zhou, 1996). This is important, because the lateral variations in lithology seem to control the depth extents, and thus the magnitudes, of potential future earthquakes (Magistrale and Zhou, 1996). These depths, which may correlate with the presence of schist basement rocks (Pelona schist in this case), can be determined from the depth of the current background seismicity and from seismic images like those of Fig. 4.4A.

Fig. 4.4A shows the depth migration of records from 18 events, including the Sierra Madre main shock, using the southern California velocity model of Fig. 3.1 for traveltimes computation. The data set included as few as 18 and as many as 102 seismograms from each event, all having impulsive P -wave picks. Most of the focal mechanisms for these events show thrust faulting (Hauksson, 1994) and their depth distribution lies between 8.3 and 14.1 km. Datum is sea level. Brown (or dark shading) shows positive reflectivity, white shows negative reflectivity and yellow (or light shading) shows small reflectivity.

To test the validity of my image, I must determine which imaged structures are real and which are artifacts produced from the imaging of noisy data. One test is

ch4f4.ps

a simple resampling analysis, which is done by imaging the data after destroying coherence by randomly flipping the signs of data traces. Fig. 4.4B depicts migration artifacts and is equivalent to migration of random noise. Compare with Fig. 4.4A to visually separate out artifacts from the signal of coherent reflectors. The images are most prominently different at the LCRZ. Note how the San Andreas fault seems to extend nearly vertically through the upper crust, despite the presence of nearby imaging artifacts (Fig. 4.4B). However, its reflectivity is not as strong as that of the LCRZ.

Fig. 4.4A suggests the reflective bright spot of Fuis et al. (Fig. 4.4C) extends north beneath the San Andreas fault to the Mojave Desert. My Sierra Madre migration shows, among the usual elliptical Kirchhoff migration artifacts, a strong north-dipping reflective zone at approximately 10-20 km depth below the northern side of the San Gabriel Mountains. Fig. 4.4B shows some negative image of the northern end of the LCRZ, indicating I should have less confidence in its existence than in the main section of the LCRZ.

Fig. 4.4D overlays the LARSE Line 1 stack of Fuis et al. (1996) on my migration at the same scale, assuming the stack was created with accurate enough velocities to avoid vertical exaggeration, and at approximately corresponding locations. Assuming that the bright spot is larger than 10 km, the locations of the bright spot reflector on the two sections correspond well, despite the fact that the sections are not coincident.

One way of visualizing how migrations of each event contribute to the final

depth section (Fig. 4.4A) is through a common-image gather in the imaging volume. Fig. 4.5 shows the imaging volume of the 18 events used. Note the coherent energy that contributes to the most prominent reflector, the LCRZ.

4.3.2 Northridge earthquake sequence

A major debate in the Los Angeles basin region, analogous to that commonly found in deep seismic profiling (e.g., Cook and Varsek, 1994), has centered around the question of whether blind thrust faults maintain a constant dip and thus penetrate into deep basement (“thick skin tectonics”), or whether such faults flatten above or into a regional, subhorizontal detachment horizon, or *décollement*, above or high in the basement (“thin skin tectonics”). Seismological evidence for the Northridge mainshock faulting, the focal mechanism, and the spatial distribution of aftershocks (Hauksson et al., 1995) together with geologic and geodetic constraints (Donnellan et al., 1993), are consistent with both “thin-” (Davis and Namson, 1994) and “thick-skinned” (Yeats, 1993; Huftile and Yeats, 1996) hypotheses for blind-thrust faulting in southern California.

The presence or absence of a mid-crustal detachment in the western Transverse Ranges is a subject of current debate (Webb and Kanamori, 1985; Yeats, 1993; Davis and Namson, 1994; Huang et al., 1996; Huftile and Yeats, 1996). Huang et al.’s (1996) analysis of low-angle earthquake focal mechanisms does not support the existence of a regional-scale, seismically active detachment in southern California. Only in the western Transverse Ranges is there some suggestion of a large

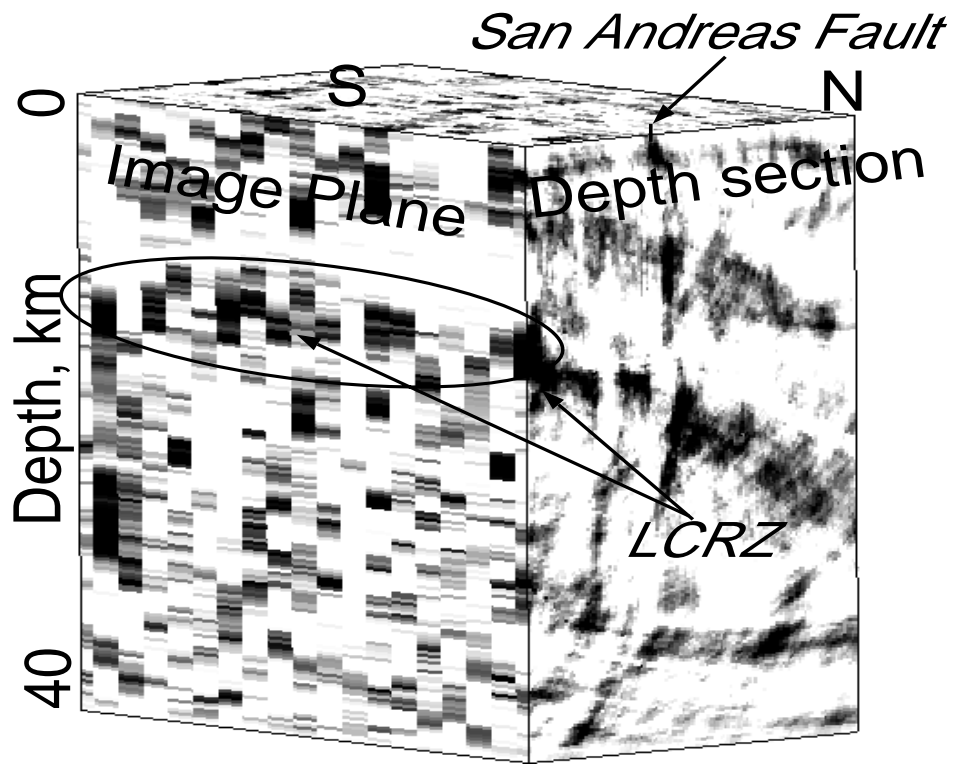


Figure 4.5: Imaging volume showing migrations of all traces from each of the 18 events used, on the left face of the volume. The left represents the image plane, over which horizontal summation produces the final depth section on the right. Note the coherent energy that contributes to the LCRZ in the final depth section.

detachment surface at a depth of about 13 to 14 km (Huang et al., 1996). Davis and Namson (1994) proposed that a detachment lies at a depth of about 22 km.

One way to refine these alternative models is to use aftershock recordings to attain crustal images. This is needed because the “thin-skinned” and “thick-skinned” interpretations of the 1994 Northridge earthquake are especially dependent on accurate characterization of complex fault geometries (Mori et al., 1995). Using Suppe and Medwedeff’s (1984) techniques to model local well and geologic data, Davis and Namson (1994) proposed a model of thrust ramps along blind thrusts below the San Fernando Valley.

I can test this model using crustal reflection images. Fig. 4.6A shows an imaged crustal section 50 km wide and 40 km deep that extends north from the Northridge epicentral area (Fig. 4.1, line B; the N-S orientation of section B allows me to compare my results with available information, and is also for computational convenience). The imaging utilizes the southern California velocity model of Fig. 3.1 and 823 wide-angle seismograms having high-quality impulsive P -wave picks from 27 shallow Northridge aftershocks. Nearly all of the focal mechanisms for these events show thrust faulting (Hauksson et al., 1995) and their depth distribution lies above 3 km. Datum is sea level. Black shows positive reflectivity, white shows negative reflectivity, and gray shows little reflectivity.

Strong, north-dipping reflectors, and one south-dipping reflector, in Fig. 4.6A do not follow the trajectories defined by the artifacts of Fig. 4.6B. They correlate closely with Davis and Namson’s (1994) interpreted positions of the Pico and

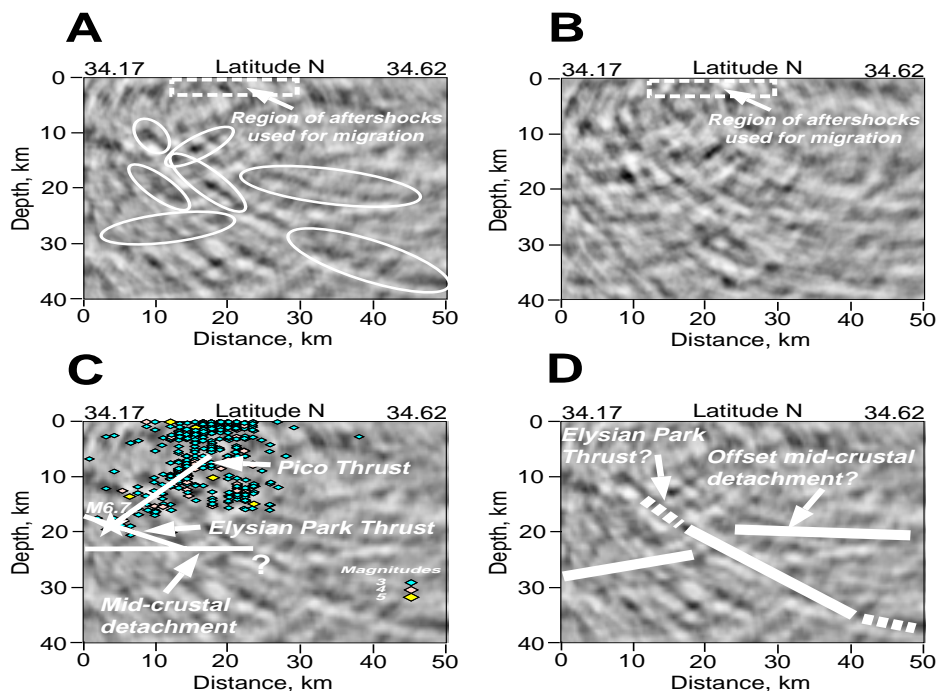


Figure 4.6: A) Crustal reflectivity below the Northridge sequence along a south-north section (Fig. 4.1, line B). The image has contributions from 27 A-quality aftershocks lying within 3 km of the surface. It was dip-filtered (Hale and Claerbout, 1983) to enhance the main reflectors. Note the north-dipping fault system and a south-dipping reflector. B) Depth section based on a simplified resampling analysis. This image depicts migration artifacts and is equivalent to migration of random noise. Compare with (A) to visually separate out artifacts from signal (coherent reflectors). C) Same image as in (A) with Northridge main shock, aftershocks and interpretations of Davis and Namson (1994) superimposed. Dipping reflectors appear that may correspond to the Pico and Elysian Park thrusts, but they extend below the projected 22 km depth of the mid-crustal detachment. D) Same image as in (A) showing my interpretation. This is based on coherent reflections and existing geologic data. Lines suggest the approximate location of an offset mid-crustal detachment and a north-dipping fault that may correspond to the Elysian Park thrust as inferred by Davis and Namson. The Moho interface is located at 32 km.

Elysian Park Thrusts, but the reflectors extend below the projected depth of their proposed mid-crustal detachment. Fig. 4.6B displays migration artifacts and is equivalent to migration of random noise in the same manner as that in Fig. 4.4B. Note how the prominent north-dipping fault system and the south-dipping reflector do not appear, and therefore are not imaging artifacts. Compare with Fig. 4.6A to visually separate out artifacts from signal (coherent reflectors).

This is one way of establishing the validity of specific points that I interpret as within coherent reflectors (within the white ellipses of Fig. 4.6A). For instance, some points of the south-dipping reflector (at about 15.5 km distance, 13.1 km depth), the north-dipping reflector (at about 17.6 km distance, 20.0 km depth), and one nearly-horizontal reflector (at about 40.0 km distance, 21.7 km depth) do not look the same in the noise estimate (Fig. 4.6B). One can also define specific points of artifacts in an analogous way, but they look alike and negated, as discussed in Chapter 3.

Fig. 4.6C compares my wide-angle SCSN data image with aftershock locations, and with part of Davis and Namson's (1994) balanced cross section. A south-dipping reflector, depicted in Fig. 4.6A, just below their Pico Thrust may be an image of the seismogenic fault. Note that my image also shows a dipping reflector almost parallel to the main north-dipping reflector.

Fig. 4.6D shows my interpretation of the image in Fig. 4.6A. It depicts faults based on coherent arrivals (as compared with Fig. 4.6B). Subhorizontal reflectors visible at mid-crustal depths (between 20 and 28 km) may be evidence for a large

subhorizontal discontinuity, perhaps a detachment fault. This feature is apparently offset by the north-dipping thrust that may correspond to the Elysian Park thrust. Note that the thrust is steep, cuts the mid-crustal detachment and crust-mantle boundary (at 32 km), and appears to pass beneath the San Andreas fault and root to the north. This suggests that the present crustal shortening in the region involves both the lower and upper crust.

It is also convenient, for the sake of visualizing how migrations of each event contribute to the final depth section, to take a look at a common-image gather in the imaging volume. Fig. 4.7 shows the imaging volume of the 27 events used. Note the coherent energy that contributes to two of the most prominent reflectors, the offset mid-crustal detachment (?) and the Elysian Park Thrust (?). Compare with Fig. 4.6D for the location of interpreted structures.

4.4 Discussion and conclusions

The agreement between my depth section through the San Gabriel Mountains and that of the LARSE Line 1 is a positive test of my crustal imaging work. It is remarkable that the dense 2-D LARSE Line 1 explosion data and the very wide-angle, sparse 3-D aftershock network records can show the same bright spot extending north from the San Gabriel Mountains area, beneath the San Andreas, and into the Mojave.

This fact suggests not only that the lower crustal reflective zone is real, but

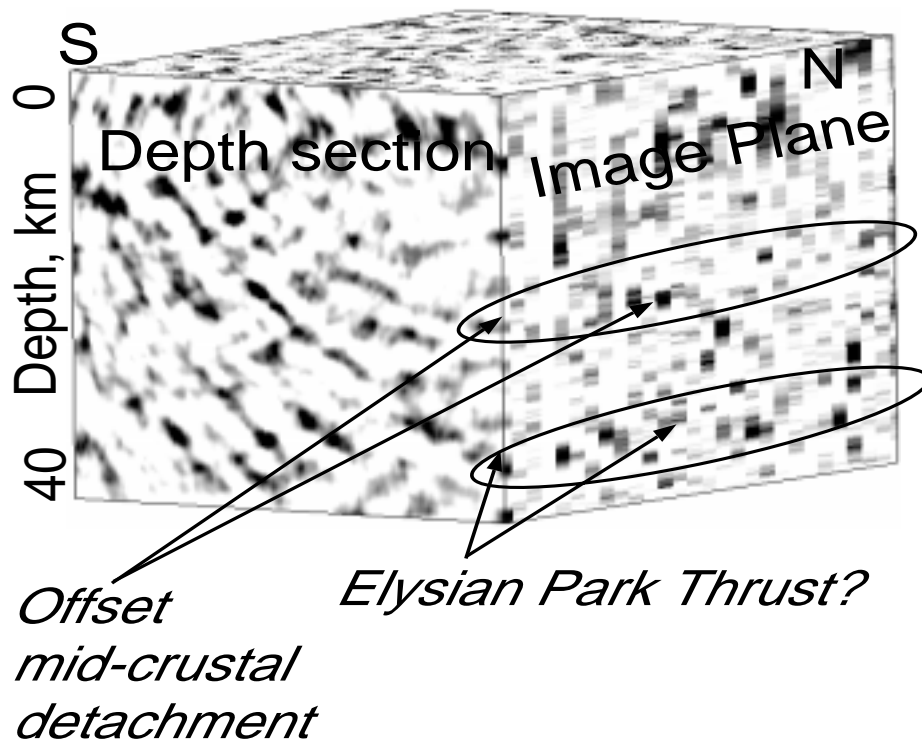


Figure 4.7: Imaging volume showing migrations of all traces from each of the 27 events used, on the right face of the volume. The right represents the image plane, over which horizontal summation produces the final depth section on the left. Note the coherent energy that contributes to the definition of two of the interpreted features in the final depth section.

also supports the accuracy of both data sets and imaging methods. Unfortunately, no other geophysical data are available to corroborate the locations of reflective structures at depths greater than 4 km, which are below the reach of petroleum industry seismic and borehole data in southern California. LARSE Line 1 results to date have provided useful information on the tectonics of southern California (Fuis et al., 1996), but have not yet shown clear structural definition of faults. However, I have shown here that it is possible to image fault geometry beneath the northern margin of the Los Angeles basin using earthquake sequences.

My results from Northridge do not support the “thin-skinned” interpretation of Davis and Namson (1994). My image suggests that the main, north-dipping thrust (Elysian Park thrust?) is steep, cuts a mid-crustal detachment and the crust-mantle boundary, and appears to pass beneath the San Andreas fault and to root to the north. This thrust appears to be similar to the deeply-penetrating Flannan Thrust in Britain (Brewer and Smythe, 1983; Brewer et al., 1983; Blundell, 1990), which, in deep reflection images, appears to cut the crust-mantle boundary.

For the last 17 years, the literature regarding this region has mostly favored the “thin-skinned” model (e.g., Huftile and Yeats, 1995). My interpretation is more consistent with a “thick-skinned” tectonic regime. This suggests that the present crustal shortening in the region involves both the lower and upper crust.

The main difference between my results from Sierra Madre and those from Northridge arises mostly from their different source illumination. Sierra Madre aftershock locations make allowance for a successful illumination of mid-crustal

reflectors (like the LCRZ) mostly with forward-scattered energy (in this case one cannot choose shallow events to illuminate reflectors with backscattered energy). Illumination is restricted to the left and below reflecting structures like the LCRZ. On the other hand, the Northridge aftershock locations I used illuminate deep reflectors with backscattered energy. This allows me to define much deeper structures (like the Moho) and interpret more features despite its lower (overall) image quality and resolution.

Given the high cost of active source crustal imaging, together with the difficulty of working in heavily populated areas, my new crustal imaging technique provides a practical means to improve our understanding of the geometry of active faults in southern California. I can image thrust geometry and other structures extending into the lower crust, although data limitations will continue to be a major hurdle. The station distribution of the SCSN is inadequate to resolve faults throughout southern California; such work will be restricted to aftershock zones.